Analysis of Au–Pd driving forces via the effective site energy model: LRO, antisites and enthalpy of permutation

F Berthier, B Legrand

PAPER

Analysis of Au–Pd driving forces via the effective site energy model: LRO, antisites and enthalpy of permutation

View the article online for updates and enhancements.

Analysis of Au–Pd driving forces via the effective site energy model: LRO, antisites and enthalpy of permutation

F Berthier[1,3] and B Legrand[2]

[1] Université Paris-Saclay, CNRS, Institut de chimie moléculaire et des matériaux d'Orsay, 91405, Orsay, France
[2] Université Paris-Saclay, CEA, Service de Recherches de Métallurgie Physique, 91191, Gif-sur-Yvette, France

E-mail: Fabienne.Berthier@universite-paris-saclay.fr

CrossMark

Abstract

Recently we have developed a new energetic model based on the determination of the energies on each site of random solid solutions after relaxation as a function of both the local composition and the nominal concentration. It allows to determine the main thermodynamics driving forces of disordered alloys. Here, we extend the effective site energy model to ordered alloys and illustrate the results for the Au_cPd_{1-c} system. As a first step, we show the ability of this energetic model to reproduce the hierarchy of ordered phases. Then, we derive general mean-field analytic formulae for ordered systems and get the phase diagram. We determine the relative role of the cohesive effect, the chemical effect and the size effect and find that the chemical effect differs significantly between the disordered state and the ordered state. Finally, we link the energy formation of antisite to the permutation enthalpy and give the driving forces for the formation of antisite.

Keywords: phase diagram, driving forces, LRO, site energy, antisite, permutation enthalpy, AuPd

(Some figures may appear in colour only in the online journal)

1. Introduction

Although phase diagram of bimetallic alloys are well documented, the driving forces that drive the thermodynamic are not as often studied. In the disordered state the thermodynamic forces are the cohesive effect, the chemical (or alloying) effect, the elastic (or size) effect [1, 2]. The cohesive effect is generally the main effect for segregation phenomena [3] whereas the interplay of the chemical and elastic effects dominate the thermodynamics of phase diagrams [2, 4]. So far, these contributions have mostly been determined within the limits of dilution [2, 5]. We have recently developed an original model which allows the determination of these driving forces on the whole concentration range. This method is based on the determination of site energies of random solid solutions (RSS) of which

atomic positions are relaxed using semi-empirical interatomic potentials. The originality of this approach is to extract site energies for each specie of the alloy according to local composition and nominal concentration. So far we have used this model to study alloys in the disordered state, i.e. at very high temperatures [6], and when short-range order (SRO) is present in disordered state i.e. at high temperatures [7]. Right now we apply the effective site energy (ESE) model to the Au_cPd_{1-c} alloy at low temperature when long-range order (LRO) occurs.

Within the ESE model we start from the disordered state and we attempt to describe the ordered structures. Therefore it is a reverse approach of the cluster expansion (CE) [8, 9] which starts from the ordered structures and then expects to be able to process the disordered alloy as well. Another difference lies in the fact that for the CE, the energies of ordered structures are derived from *ab initio* calculations, whereas the calculation of site energies is not always possible in *ab initio*, in any

---

case it is not commonly developed [10, 11]. The approach presented is in fact possible because site energies can be obtained from semi-empirical potentials. Nevertheless, semi-empirical potentials have rarely driven site energy analyses, as the result of simulations is most often preferred to driving force analysis.

The permutation enthalpy (or enthalpy of transmutation) which corresponds to the enthalpy variation linked to the permutation of a B atom into an A atom for an A_cB_{1-c} alloy, is the crucial quantity that controls phase diagrams and interfacial segregation [6, 7]. Thanks to site energies, an analytical expression is obtained. It involves the partial derivatives of the site energies with respect to the local composition on the one hand and with respect to the nominal composition on the other hand. This separation of terms allows to split up the permutation enthalpy into three components, namely the cohesive, chemical and elastic effects. In addition, this approach makes it possible to characterize and understand differences with the Ising model, which is based on constant interaction energies, or with models based in interactions that depend on concentration. This method is therefore a very powerful analytical tool.

To illustrate this approach, we have chosen the AuPd system, which we have already studied previously [7, 12]. This system has been the subject of many studies because it has good catalytic properties [13–15]. AuPd is an alloy with a weak tendency to order and a strong difference in size parameter ($\Delta r/r = 6\%$). It forms a RSS with a fcc structure at high temperature over the whole concentration range. At low temperatures, AuPd is subject to many debates, studies giving various results. AuPd has a negative mixing enthalpy on the entire temperature range [16], which is the signature of an alloy with a tendency to order, but the stability domains of the ordered phases are hypothetical [17]. Three ordered phases are predicted at low temperature at $c = 0.25$, $c = 0.5$ and $c = 0.75$. Depending on the studies, and according to the object considered experimentally (bulk, thin film or nanoparticle) or the numerical method used (CE starting from *ab initio* calculations via GGA or LDA...), the results differ on the most stable structures between the structures $L1_2$, DO_{22}, DO_{23} and between the structures A_2B_2 and $L1_0$ [18–27].

In ordered phases one question concerns the concentration of point defects such as antisites, vacancies, and complex defects. In this matter, a lot of research effort has been involved over the last decades in the study of alloys [28–32]. It is challenging to predict the equilibrium of antisites, therefore the Wagner–Schottky model is the simplest and most commonly used [33]. In perfectly ordered structures, atoms A and B occupy the sites of different sublattices. Different types of defects have been considered: atoms A and B on interstitial sites (which are often insignificant); vacancies in the sublattices of components A and B; and finally atoms A on sites of the sublattice rich in atoms B and atoms B on sites of the sublattice rich in atoms A. This model assumes that point defects are non-interacting and that the formation energy, which is the central quantity, depends linearly on the concentration. Energies are calculated by either semiempirical or *ab initio* calculations [34, 35]. When the concentration of defects

is relatively high, such as in AuCu, it is better to consider the Bragg–Williams [36] or single-site mean-field model [37]. Moreover, when the antisites are strongly preponderant over the vacancies, the equilibrium solution can be obtained from the determination of isotherms based on the permutation of atomic species [38] but to our knowledge the link between the formation energy of antisite and the enthalpy of permutation has not yet been studied.

We use N-body interatomic potentials from the second moment approximation (SMA) adjusted on *ab initio* calculations [7, 12]. The purpose of this paper is not a new study on the stability of ordered phases and on the values of critical temperatures but on the application of site energies to predict ordered alloys. We are therefore exploring the coherence between SMA simulations and the formalism of site energies. After a first step to validate the use of site energies for ordered state, the core of this work is the determination of the driving forces that control low-temperature thermodynamics when LRO occurs. For this purpose, we extend the mean field formalism based on site energies to discriminate the cohesive, alloying and size effects. Because the system is heterogeneous, it is necessary to introduce sublattices. This formalism leads to the determination of the phase diagram via isotherms. Isotherms are used to quantify antisites as a function of the concentration and temperature. We then expressed the energy of antisite formation as a function of site energies and compared the driving forces of the phase diagram with those of antisite formation, which has never been done before.

The work is organized as follows. In section 2 we present the mean field formalism, based on site energies, developed for a homogeneous system and its extension to heterogeneous systems with LRO. Section 3.1 describes the site energies, the formation energies of ordered structures and the effective pair interaction of the alloy. The isotherms and the phase diagram are presented in section 3.2 before discussing the enthalpy of permutation and its decomposition into three components. Section 3.4 presents the analysis of the enthalpy of permutation in the case of phase $L1_0$, and the link with the formation of antisites. Finally, we present our conclusions in section 4.

2. Model

Before detailing the evolution of the system, we describe the energetic model and the numerical methods used.

2.1. Energetic model

Starting from N-body interatomic potentials derived from the second moment approximation of tight-binding scheme [39], we calculate the energies of the Pd and Au atoms after relaxation of the atomic positions using the FIRE algorithm [40]. To obtain site energies according to their different local composition and nominal concentration, all possible environments are considered in first neighbours of a given atom, the rest of the box being in chemically disordered configurations of a given concentration. The site energy is the average of all site energies of atoms having the same local environment as the chosen

atom. The site energies (noted E_X^p with X = Au, Pd) therefore depend on the local composition (characterized by the number p of first neighbours of type Au but it would also be possible to consider the number of first neighbours of type Pd) and the nominal concentration c (due to size-misfit between both constituents).

We define a rigid lattice formalism to describe an alloy $A_c B_{1-c}$ (in this case the alloy $Au_c Pd_{1-c}$). The following Hamiltonian gives the internal energy as a function of site energies:

$$H = \sum_{i=1}^{N_{at}} \left(p_i E_A^{\sum_{j \in v_i} p_j} + (1 - p_i) E_B^{\sum_{j \in v_i} p_j} \right) \qquad (1)$$

where N_{at} is the total number of atoms, p_i the occupation factor of site n: it is equal to 1 if site n is occupied by an Au atom and 0 if not; and v_i represents the set of first-neighbors of site i.

This Hamiltonian can be introduced into Monte Carlo (MC) simulations or mean field formalism (MF). To take full advantage of the analytical approach, in particular for the analysis of permutation enthalpies, we have chosen to favor the mean field approach over Monte Carlo. Indeed, obtaining the exact phase diagram in SMA or within site energies is not a problem and is not the subject of this article.

Remember that this rigid lattice formalism takes into account relaxations in RSS but of course, as for any rigid lattice formalism, it does not allow to treat the case of a lattice change, for example a B2 phase on bcc structure in relation to a RSS fcc structure.

2.2. Mean-field approximation

The Hamiltonian (1) of a homogeneous system is written in the mean field approximation

$$H = N_{at} \left(c E_A^{Zc} + (1 - c) E_B^{Zc} \right) \qquad (2)$$

where Z represents the coordination number.

In the grand canonical ensemble, the free energy F is given by $F = H - TS - c N_{at} \Delta \mu$, where T is the temperature and S is the configurational entropy that is written in the Bragg–Williams approximation [36]:

$$S = -k_B N_{at} \left(c \, ln \, c + (1 - c) \ln (1 - c) \right) \qquad (3)$$

with k_B the Boltzmann constant.

The equilibrium concentration is obtained by minimizing the free energy $\partial F / \partial c = 0$:

$$\frac{c}{1 - c} = \exp \left(-\frac{\Delta H^{perm} - \Delta \mu}{k_B T} \right). \qquad (4)$$

As we can see from equation (4), ΔH^{perm} is the cornerstone of isotherms. The enthalpy of permutation corresponds to the energy change when a B atom is switched to an A atom:

$$\Delta H^{perm} = \frac{\partial H}{N_{at} \partial c}. \qquad (5)$$

ΔH^{perm} is calculated by derivating equation (2) which leads to the expression:

$$H^{perm} = \left(E_A^{Zc} - E_B^{Zc} \right) + Z \left(c \left. \frac{\partial E_A^p}{\partial p} \right|_{Zc} + (1 - c) \left. \frac{\partial E_B^p}{\partial p} \right|_{Zc} \right)$$
$$+ \left(c \left. \frac{\partial E_A^p}{\partial c} \right|_{Zc} + (1 - c) \left. \frac{\partial E_B^p}{\partial c} \right|_{Zc} \right). \qquad (6)$$

The enthalpy of permutation is therefore the sum of three terms:

- The first term on the RHS corresponds to the energy variation on the site where a B atom is permuted into a A atom.
- The 2nd term on the RHS corresponds to the energy variation of the Z nearest-neighbours sites of the site on which the exchange occurs.
- The 3rd term on the RHS corresponds to the energy change of the system when the concentration goes from c to $c + 1/N_{at}$. It is therefore an elastic term linked to the variation of the lattice parameter due to the concentration variation.

Thus this method allows deriving an analytical expression of the permutation enthalpy over the entire concentration range for RSS and possibly with SRO [6, 7], whereas until now the permutation enthalpies were calculated only within the infinitely diluted limits [2, 5]. What about when there is LRO? In the case of ordered phases, the system is heterogeneous and it is no longer possible to directly use the mean field approximation to the entire system. However, it can be used by considering nsr sublattices of composition c_i, each sublattice being homogeneous. The formalism presented above is then applied to each sublattice (see appendix A) leading to a non-linear system of coupled equations:

$$\frac{c_i}{1 - c_i} = \exp \left(-\frac{\Delta H_i^{perm} - \Delta \mu}{k_B T} \right), \qquad (7)$$

where ΔH_i^{perm} is the permutation enthalpy of the sublattice i. It corresponds to the energy balance when a B atom of sublattice i is switched to an A atom:

$$\Delta H_i^{perm} = \frac{\partial H}{\partial N_{Ai}} = \frac{nsr}{N_{at}} \frac{\partial H}{\partial c_i}. \qquad (8)$$

The permutation enthalpy of the system is then written according to the permutation enthalpies of the different sublattices:

$$\Delta H^{perm} = \frac{1}{nsr} \sum_{i=1}^{nsr} \Delta H_i^{perm} \frac{\partial c_i}{\partial c}. \qquad (9)$$
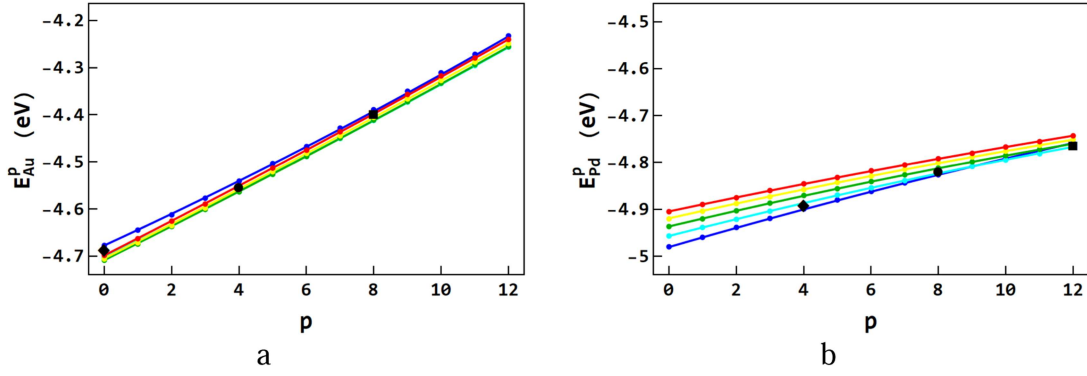
We thus obtain a simple analytical expression of the enthalpy of permutation for an alloy with LRO.

3. Results

3.1. Energetic model

It is interesting to compare the main characteristics of the site energies with those of a standard Ising model with

Figure 1. Site energy of an atom I = Au (a), Pd (b), as a function of the number p of Au neighbours, for different values of the concentration in Au_cPd_{1-c} alloy (blue: $c = 0$, cyan: $c = 0.25$, green: $c = 0.5$, yellow: $c = 0.75$ and red: $c = 1$). The lines are only a guide for the eyes. Values of site energies of the ordered structures are indicated: $L1_2$ at $c = 0.25$ (diamonds), $L1_0$ at $c = 0.5$ (dots), $L1_2$ at $c = 0.75$ (squares).

Table 1. Formation energies E_{form}^{SO} and ordering energies E_{mO}^{SO} of the ordered structures. Comparison between the direct SMA calculation, and calculation using the site energies considering only the nearest-neighbour shell E_X^p or the site energies in 1st and 2nd neighbouring $E_X^{p_1,p_2}$.

|	$c = 1/4$		$c = 1/2$		$c = 3/4$	
	$L1_2$	DO_{22}	$L1_0$	A_2B_2	$L1_2$	DO_{22}
E_{form}^{SO} (meV/at)						
SMA	−44	−45.5	−76	−79	−64.7	−66
E_X^p	−45	−45	−77.5	−77.5	−66.5	−66.5
$E_X^{p_1,p_2}$	−47.25	−47.5	−76.5	−80	−63.5	−64.5
E_{mO}^{SO} (meV/at)						
SMA	−11.83	−13	−21.96	−25	−18.41	−20
E_X^p	−13.25	−13.25	−23	−23	−19.7	−19.7
$E_X^{p_1,p_2}$	−14.5	−14.75	−22	−25.7	−17.5	−19

interactions between first neighbours (V_{AA}, V_{BB}, V_{AB}). For a given concentration, site energies are not linear functions of the local environment: the curve of an Au atom is slightly concave (figure 1(a)) and that of a Pd atom is convex (figure 1(b)). This behaviour differs from that of an Ising model for which the energy of an atom A varies linearly with the number p of nearest neighbours of type A according to $(pV_{AA} + (Z − p) V_{AB})/2$, and for an atom B according to $(pV_{BA} + (Z − p) V_{BB})/2$. The second difference is that site energies depend on the nominal concentration whereas in a conventional Ising model the interaction energies are constant.

The site energies in the ordered structures are slightly less cohesive than in the disordered state for Au atoms (figure 1(a)) and slightly more cohesive for Pd atoms (figure 1(b)). Even if the deviations are small, it is therefore questionable whether it is reasonable to consider site energies that are average values obtained for a disordered environment to apply them to ordered systems? We therefore checked the ability of the site energies to reproduce the energies of the ordered structures obtained directly via the SMA. The formation energies of the ordered structures E_{form}^{SO} and ordering energies E_{mO}^{SO} obtained in SMA are compiled in table 1. The values of the formation energies and of the ordering energies are negative, indicating respectively a stability of the ordered phases as compared to pure metals and to RSS. The $L1_0$ structure is more stable than the $L1_2$ structure at $c = 0.75$ which is itself more stable than the $L1_2$ structure at $c = 0.25$. The values from the site energies are

very close and the hierarchy is perfectly reproduced. We obtain that DO_{22} and A_2B_2 structures are respectively the most stable structures in SMA (table 1). Structures $L1_0$ and A_2B_2 and structures $L1_2$ and DO_{22} are not differentiated by the nature of nearest neighbours. Thus we have calculated their formation energies with site energies taking into account the dependence with the chemical nature of the first and second neighbours $E_X^{p_1,p_2}$. We show that DO_{22} and A_2B_2 structures are respectively more stable than $L1_2$ and $L1_0$ structures (table 1). The formation or ordering energies of the ordered structures calculated from the site energies of the second neighbours are in good agreement with the SMA values; the stability hierarchy of the structures is correctly reproduced. It can be noted that these results are in agreement with those obtained from the CE calculations [13, 14] but this is not the subject of this study as we are mainly focused on the consistency between the SMA and the site energies.

The site energies restricted to the nearest-neighbouring shell for their dependency on the local environment are sufficient to reproduce the hierarchy of the formation and ordering energies of the ordered phases $L1_2$ and $L1_0$. We therefore limit the study to the first neighbours to simplify the formulas and facilitate the reading, the object of the article being the analysis of the driving forces of a system with LRO.

From the site energies we determine the effective pair interactions that drive the local ordering. The site energies presented in figure 1 are written as the sum of a linear term and

4
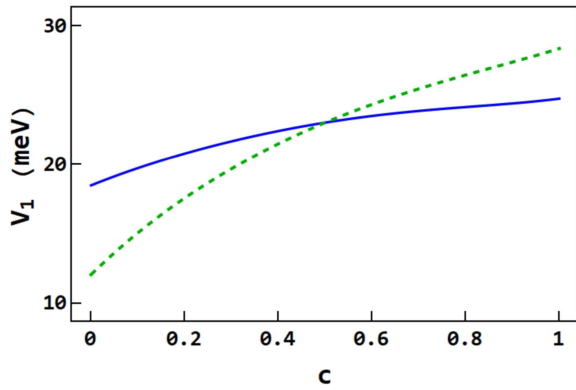
Figure 2. Evolution of the nearest-neighbor effective pair interaction V_1 with the concentration c when the curvature of the site energies is not taken into account V_1^{Ising} (blue) and when it is V_1^{χ} (green, dashed).

a quadratic term according to the chemical composition of the nearest neighbours:

$$E_X^p(c) = E_X^0(c) + \frac{p}{Z}\left(E_X^Z(c) - E_X^0(c)\right) + \chi_X p(Z - p) \quad (10)$$

where χ_X stands for the curvature of X with X = A or B. The linear term allows to recover the Ising model with the pair interactions which in this case depend on the concentration. For $p = 0$ and $p = Z$, the site energies of the two types of atoms are written simply as a function of the pair interaction energies: $E_A^Z(c) = Z\frac{V_{AA}(c)}{2}$, $E_A^0(c) = Z\frac{V_{AB}(c)}{2}$, $E_B^Z(c) = Z\frac{V_{BA}(c)}{2}$ and $E_B^0(c) = Z\frac{V_{BB}(c)}{2}$. At a given concentration, the difference between the two slopes leads to the expression of the first neighbours effective pair interactions $V_1^{\text{Ising}}(c)$:

$$ZV_1^{\text{Ising}}(c) = \left(E_A^Z(c) - E_A^0(c)\right) - \left(E_B^Z(c) - E_B^0(c)\right). \quad (11)$$

Taking into account the curvature, which is not zero as a function of p, induces a variation in the effective alloying interactions with the local concentration, which in turn depends on the nominal concentration:

$$V_1^{\chi}(c) = \left(\left.\frac{\partial E_A^p}{\partial p}\right|_{Zc} - \left.\frac{\partial E_B^p}{\partial p}\right|_{Zc}\right). \quad (12)$$

As expected for the AuPd alloy, the nearest-neighbour effective pair interaction is positive, reflecting the trend to the ordering of the alloy (figure 2). The effective pair interaction V_1^{Ising} increases with concentration, this dependence is mainly elastic effect related to the variation of the lattice parameter with c. Taking into account the curvature leads to a variation of the effective pair interaction V_1^{χ} of about 15 meV instead of 5 meV for V_1^{Ising} when one passes from Pd(Au) to Au(Pd). This chemical effect is one of the reasons of the hierarchy of critical temperatures of the ordered phases.

3.2. Mean field isotherms

As mentioned above, we consider a first neighbour approach. We have previously shown that in this case the ordered phases $L1_0$ and $L1_2$ are stable. Phase $L1_0$ is characterized by an alternance of pure planes in one direction for AuPd composition.

The stoichiometric compounds $AuPd_3$ and Au_3Pd in the $L1_2$ structure are composed of a pure Pd (respectively Au) plane and a mixed Au–Pd plane. The description of these phases requires the introduction of 4 sublattices. The evolution of the concentration of each sublattice enables characterizing the long-range order of the system.

The mean field isotherms $c(\Delta\mu)$ are presented in figures 3(a)–(c) at different temperature values. At low temperatures, the isotherms have plateaux at concentrations which correspond to $AuPd_3$, AuPd and Au_3Pd compounds. Outside the plateaux, the slope of the isotherm is generally positive except for concentrations below $c = 0.25$. We have previously shown that this characteristic behaviour of phase separation is driven by the size effect [7]. We also note the presence of small S or backward returns of the isotherm for concentration values close to 0.25, 0.75 and 0.95 (figure 3(a)). The position of these S changes with temperature. When the temperature is higher, the length of the plateaux decreases, their slope increases and the S are less and less marked until they disappear. The calculation of free energy as a function of concentration shows that the S of isotherms correspond to first order transitions and determine the stable parts which are indicated by vertical lines in figures 3(d)–(f).

When the temperature increases

- The gap between the concentration of Au-rich and Pd-rich sublattices decreases;
- The concentration ranges of the $L1_2$ structures deviate from the stoichiometric composition, they shift towards $c = 0.5$. This evolution is most significant for the $L1_2$ rich in Pd;
- The structure L' which separates structures $L1_2$ and $L1_0$ at low concentrations is only observed at $T = 150$ K (figure 3(d)). The one separating structures $L1_0$ and $L1_2$ at high concentrations is observed at $T = 150$ K (figure 3(d)) and 300 K (figure 3(e));
- The domains of RSS at low and high concentrations increase.

We determine from isotherms the concentrations that delimit each phase and we report them to draw the phase diagram. Let us recall that this phase diagram includes the effects of local relaxation due to the size mismatch between the two constituents and the effects of global relaxation due to the variation in the lattice parameter (figure 4).

The most surprising result is that the phase diagram is asymmetric. Let us recall that a mean field phase diagram derived from a classical Ising model with constant pair interactions is symmetric with regard to equiatomic composition [41]. Moreover, the critical temperatures of ordered structures are expected to be equal [41]. Within this site energy model the critical temperatures of structures $L1_2$ and $L1_0$ are not equal. The hierarchy of critical temperatures is $T_c^{L1_2}(c = 0.25) < T_c^{L1_0} < T_c^{L1_2}(c = 0.75)$. These unconventional results are mainly due to the curvature term of the site energies which induces a variation in the effective pair interactions with the local and nominal concentration. The critical temperatures of the $L1_2$ structures are not obtained for compositions $c = 0.25$ or $c = 0.75$, they are switched towards the
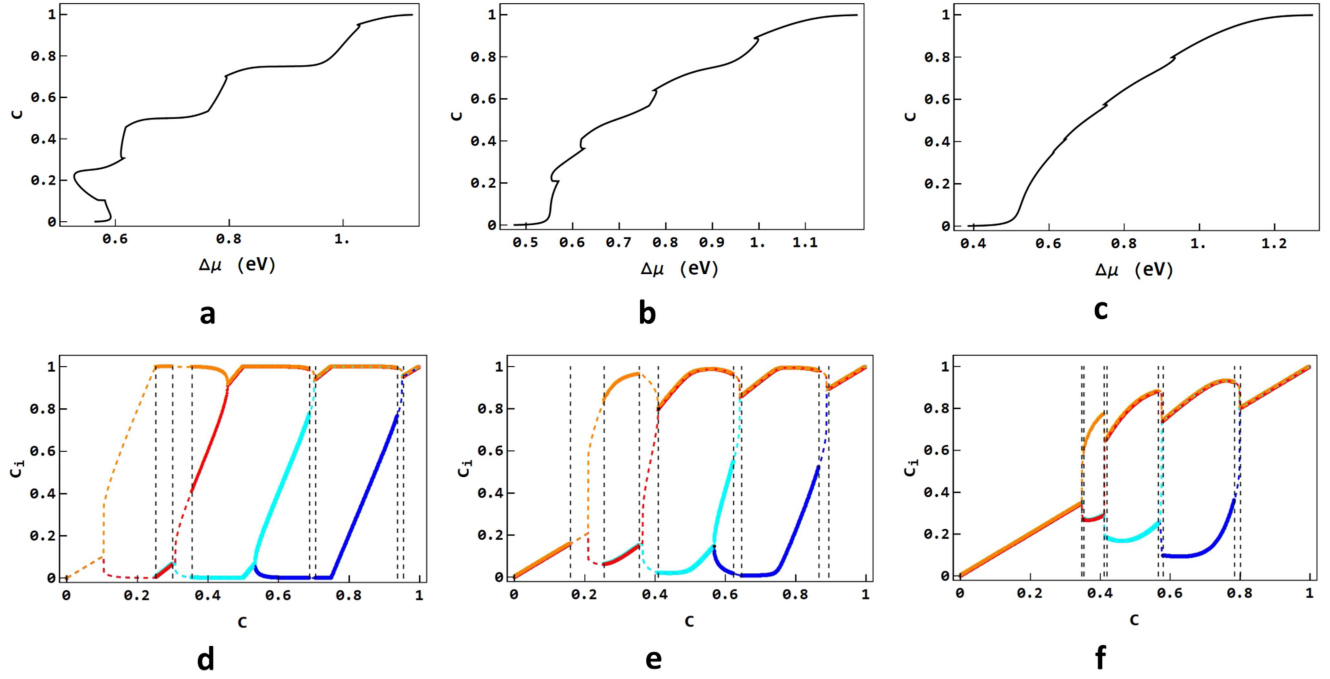
Figure 3. Mean field isotherms $c\,(\Delta\mu)$ (a–c) and c_i (c) (d–f) at $T = 150$ K (a, e), $T = 300$ K (b, d) and $T = 450$ K (c, f). Concentration of the 1st sublattice c_1 (orange), of the 2nd sublattice c_2 (red), of the 3rd sublattice c_3 (cyan) and of the 4th sublattice c_4 (blue) (d–f). The vertical dashed lines delimit the concentration ranges of the stable parts (isotherms with points) and the unstable parts (isotherms in dashed lines).
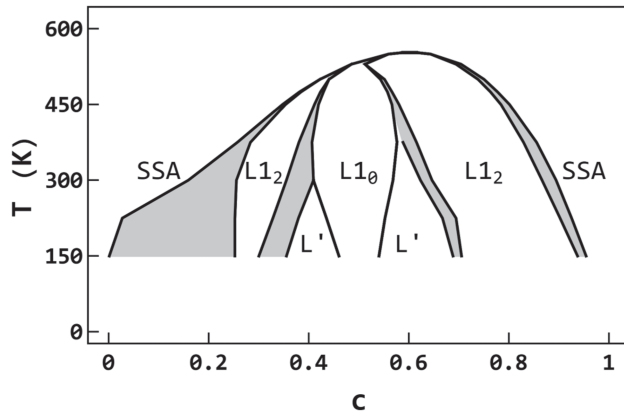
Figure 4. Phase diagram Au_cPd_{1-c}. The grey areas represent the biphased domains.
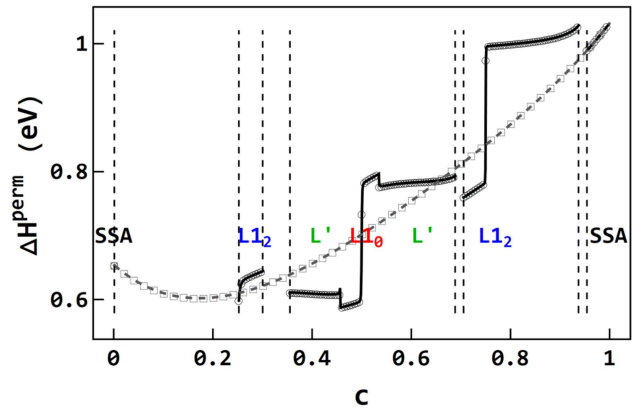
Figure 5. Comparison of $\Delta H^{\mathrm{perm}}\,(c)$ of LRO ($T = 150$ K) (continuous lines) and of RSS ($T = 1000$ K) (dashed) with also a comparison with direct calculation (symbols).

equiatomic composition, in agreement with literature for both mean field and CVM studies [41, 42].

3.3. Permutation enthalpies

3.3.1. Key role of ΔH^{perm} whatever the temperature.
The mean field formula (equation (4)) of isotherms shows that the enthalpy of permutation is the thermodynamic quantity that controls phase diagrams and more generally interfacial segregation. It corresponds to the enthalpy balance during an exchange of one B atom into one A atom (equation (5)). These relationships need to be extended for systems with LRO by defining sublattices. The permutation enthalpy of each sublattice $\Delta H_i^{\mathrm{perm}}$ is the partial derivative of the Hamiltonian with respect to c_i (equation (8)) whose analytical expression is given

in appendix A (equation (A.6)). The permutation enthalpy is the total differential of the Hamiltonian, i.e. the sum of the partial differentials according to formula (9).

Figure 5 shows the evolution of the permutation enthalpy as a function of concentration (equation (6)) for a RSS (which corresponds to the very high temperature system) and at low temperature when the system is ordered (equation (A.6)). To validate the formulae we compare the results with the direct, i.e. by calculating the energy derivative (equation (5)).

First of all, we recall that the evolution of $\Delta H^{\mathrm{perm}}\,(c)$ of a RSS is independent of temperature. Figure 5 shows that the calculation via site energies (equation (6)) is in perfect agreement with the direct calculation. ΔH^{perm} is a decreasing and then increasing function of the nominal concentration. In

the case of an Ising model, the slope of the curve gives the sign of the effective pair interaction V_1, which would mean that $V_1 < 0$ at low concentrations and $V_1 > 0$ at higher concentrations while we have shown that $V_1 > 0$ over the whole concentration range (figure 2). We have previously shown that the negative slope at low concentrations is due to elastic effects [2].

For LRO, at low temperatures, only the stable parts are displayed (figure 5). The enthalpy of permutation presents a succession of plateaux and steps. The stoichiometric compositions $AuPd_3$, $AuPd$ and Au_3Pd correspond to the steps between 2 plateaux. There are also plateaux for the phases L′. At high concentrations the curve is identical to the RSS curve. There is also a perfect agreement between the direct calculation and the analytical formula.

3.3.2. Decomposition of ΔH^{perm}. The permutation enthalpy is composed of three contributions: the first one is equal to the standard difference in cohesive energies between pure metals, the second one, known as a chemical effect, is related in a classical Ising model to the effective pair interactions and the third one, known as a size effect or elastic effect, takes into account the size misfit between the two elements. To avoid overloading the text, the formulas are detailed in appendix B in the case of RSS and for system with LRO. It should be recalled that this decomposition was validated by direct calculations within the dilute limits [2, 5].

Figure 6 shows the permutation enthalpy and its three components. The cohesive effect is independent of concentration and temperature (figure 6(a)). The size effect does not depend on temperature, it is the same for the RSS and the LRO system (figure 6(a)). The slope of the size contribution curve is first negative and then almost zero at high concentrations. The negative slope leads to the biphased domain between an almost Pd-pure RSS and the $L1_2$ structure at $c = 0.25$.

The chemical effect is very dependent on c and T (figure 6(b)). The RSS chemical contribution is an increasing function of c, so chemical and size effects are in competition. At low temperatures, in the ordered state, this curve is transformed with the presence of plateaux and steps (almost vertical parts but continuous). The chemical contribution is also the sum of two contributions, one related to the linear part of the site energies, called the Ising contribution, the other related to the curvature and called with the same name. For the disordered state, the effect of the curvature is negligible. Figure 6(b) shows that for LRO the Ising component is predominant and is at the origin of the curve's shape in plateaux and steps. The effect of the curvature is slightly more significant than for the disordered state.

The chemical effect for RSS is thus mainly related to the Ising contribution and it can be simply written as $\Delta H^{\mathrm{perm}}_{\mathrm{chem}} = 2Zc V_1^{\mathrm{Ising}}(c)$. It is no longer possible to use this classic formula for LRO, even with $V_1^\chi(c)$ instead of $V_1^{\mathrm{Ising}}(c)$. This expression cannot lead to the presence of plateaux. In the presence of LRO, the effective pair interaction $V_1^{\mathrm{LRO}}(c)$ depends on the nominal composition and local composition of the ordered structure that is considered instead of RSS. For the structure $L1_0$ for example, $V_1^{\mathrm{LRO}}(c)$ corresponds to the difference in

slopes of $E_A^4 (0.5)$ and $E_B^8 (0.5)$ instead of $E_A^6 (0.5)$ and $E_B^6 (0.5)$ for RSS (equation (C.2)).

The permutation enthalpy is driven at low temperature by the chemical contribution, which is itself controlled by the Ising contribution (figure 6(b)). The detailed analysis of this curve is the subject of the following section.

3.4. Permutation enthalpy and formation energy of antisites

3.4.1. Analysis of ΔH^{perm}. For the sake of clarity, we restrict the analysis to the case of phase $L1_0$, knowing that it is easily generalized to phases $L1_2$. Two sublattices being sufficient to describe phase $L1_0$, we can use a model with two variables c_1 and c_2 and therefore $\Delta H_1^{\mathrm{perm}}$, $\Delta H_2^{\mathrm{perm}}$ which can be written as (appendix C):

$$\Delta H_1^{\mathrm{perm}} = \Delta H_1^{\mathrm{B}\to\mathrm{A}} - 2Z_{11}V_1^{L1_0}(c) + 2(Z_{11}c_1 + Z_{12}c_2)V_1^{L1_0}(c) \tag{13a}$$

$$\Delta H_2^{\mathrm{perm}} = \Delta H_2^{\mathrm{B}\to\mathrm{A}} - 2Z_{21}V_1^{L1_0}(c) + 2(Z_{21}c_1 + Z_{22}c_2)V_1^{L1_0}(c) \tag{13b}$$

where $\Delta H_1^{\mathrm{B}\to\mathrm{A}}$ and $\Delta H_2^{\mathrm{B}\to\mathrm{A}}$ are the permutation enthalpies of the 2 sublattices at stoichiometric composition $c_1 = 1$ and $c_2 = 0$. Z_{ii} and Z_{ij} represent the intra-sublattice (resp. inter) coordination number ($Z_{ii} = 4$, $i = 1$ or 2 and $Z_{ij} = 8, i \neq j$). $V_1^{L1_0}(c)$ is the effective pair interaction for the structure $L1_0$ given by equation (C.2).

Concentrations are given by solving the equation:

$$c_1(1 - c_2) = c_2(1 - c_1)\exp\left(-\frac{2(Z_{11} - Z_{12})V_1^{L1_0}(c)(c_1 - c_2)}{k_B T}\right), \tag{14}$$

since $\Delta H_1^{\mathrm{B}\to\mathrm{A}} - 2Z_{11}V_1^{\mathrm{LRO}}(c) = \Delta H_2^{\mathrm{B}\to\mathrm{A}} - 2Z_{21}V_1^{\mathrm{LRO}}(c)$.

Isotherms issued from equation (14) are in perfect agreement with the complete model near $c = 0.5$.

We show figure 7 the evolution with the concentration of the permutation enthalpies of the two sublattices and of the full system for different temperatures. Since the plateaux are more pronounced at low temperatures, results obtained at $T = 150$ K are firstly discussed. The permutation enthalpy displays two plateaux and one step centered on $c = 0.5$ (figure 7(a)). The permutation enthalpy is equal to $\Delta H_1^{\mathrm{perm}}$ for $c < 0.5$, and to $\Delta H_2^{\mathrm{perm}}$ for $c > 0.5$, the step occurring at $c = 0.5$. According to formula (9) the permutation enthalpy is related to the sublattices permutation enthalpies via $\mathrm{d}c_1/\mathrm{d}c$ and $\mathrm{d}c_2/\mathrm{d}c$. Each plateau corresponds to a concentration range where one sublattice has a constant concentration (figure 7(d)). At low concentrations, sublattice 2 remains pure in Pd and the concentration of sublattice 1 increases linearly with the nominal concentration. Once sublattice 1 is rich in Au, its concentration is constant and the concentration of sublattice 2 increases with c. The step is almost vertical at low temperature. A temperature increase results in a decrease in the slope of the step near $c = 0.5$. The concentrations of the 2 sublattices vary simultaneously before and after the stoichiometric composition, $\mathrm{d}c_i/\mathrm{d}c$ are not constant and the permutation enthalpy is
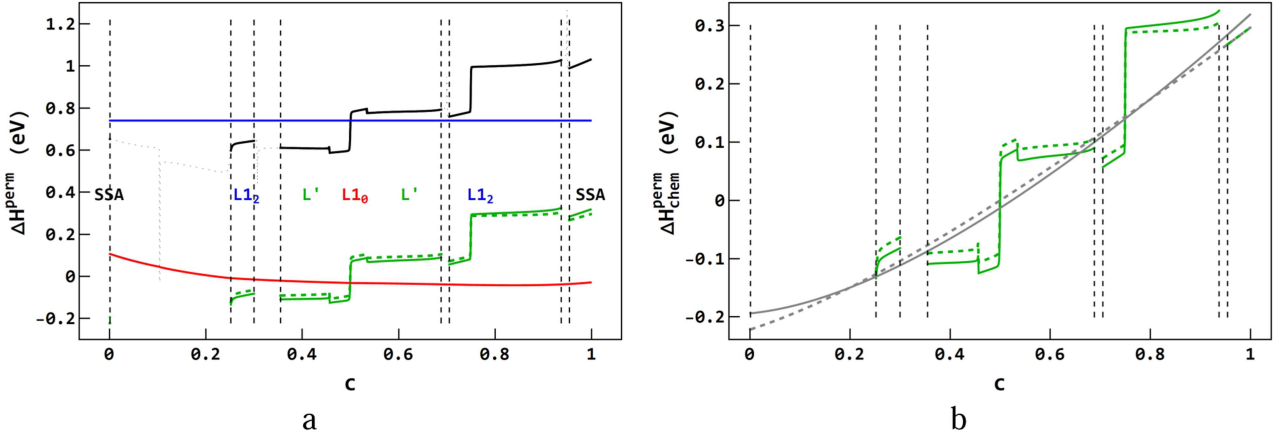
Figure 6. (a) Evolution of the driving forces as a function of c for LRO ($T = 150$ K). Black: $\Delta H^{\text{perm}}(c)$, blue: $\Delta H^{\text{perm}}_{\text{coh}}(c)$, red: $\Delta H^{\text{perm}}_{\text{size}}(c)$, green: $\Delta H^{\text{perm}}_{\text{chem}}(c)$, dashed green $\Delta H^{\text{perm}}_{\text{Ising}}(c)$. (b) Comparison of the chemical effect for LRO (green) and for RSS ($T = 1000$ K) (grey). Dashed lines represent the respective Ising contributions.
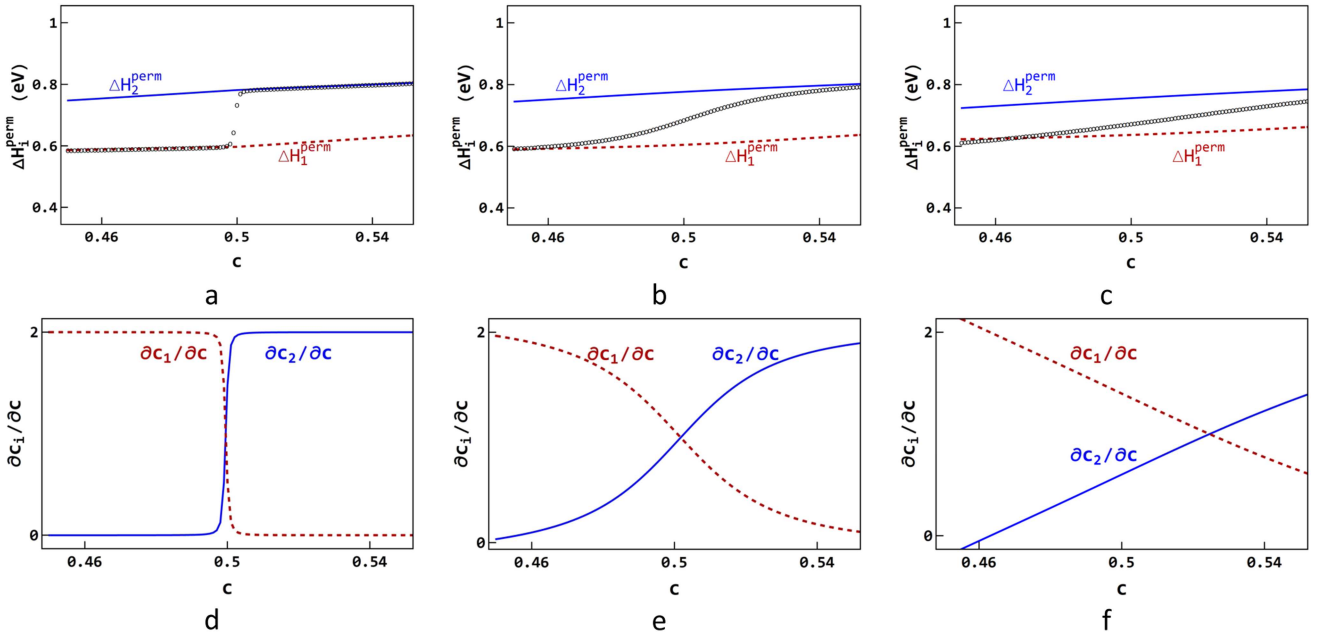
Figure 7. Permutation enthalpy of the 2 sublattices and of the total system in the concentration range of the L1$_0$ structure (a–c). Evolution of dc_i/dc with the concentration for the 2 sublattices (d–f). $T = 150$ K (a, d), $T = 300$ K (b, e) and $T = 450$ K (c, f).

no longer perfectly equal to that of a sublattice (figures 7(e) and (f)).

It can be noted that $\Delta H_2^{\text{B}\rightarrow\text{A}}$ and $\Delta H_1^{\text{B}\rightarrow\text{A}}$ can be calculated directly in SMA at 0 K by considering the energy balance after relaxation of the atomic positions during the permutation of one B atom from sublattice 2 of the L1$_0$ structure into one A atom, and of one A atom from sublattice 1 into one B atom. To keep coherence in the notations, we call permutation in the sense B $\rightarrow$ A what amounts to changing the sign of the energy balance from A $\rightarrow$ B. This leads to $\Delta H_1^{\text{B}\rightarrow\text{A}} = -\Delta E_{\text{A}\rightarrow\text{B}}$ and $\Delta H_2^{\text{B}\rightarrow\text{A}} = \Delta E_{\text{B}\rightarrow\text{A}}$. The direct calculation leads to $\Delta H_1^{\text{B}\rightarrow\text{A}} = 0.60$ eV and $\Delta H_2^{\text{B}\rightarrow\text{A}} = 0.78$ eV in perfect agreement with the values of ΔH^{perm} on each side of the step (figure 7(a)). This provides a new insight on the analysis of the $\Delta H^{\text{perm}}(c)$ curve. $\Delta H_2^{\text{B}\rightarrow\text{A}}$ and $\Delta H_1^{\text{B}\rightarrow\text{A}}$ are the energy balance between

the stoichiometric compound and the ordered structure with one antisite on one sublattice. The creation of one antisite on one sublattice defines the quasi-vertical step at the stoichiometric composition. When we deviate from the stoichiometric composition, more and more antisites are created on one of the 2 sublattices, and the permutation enthalpy is equal to the permutation enthalpy of the sublattice whose concentration varies.

The formal link between the permutation enthalpy and the formation enthalpy of antisites is the subject of the next section.

3.4.2. Formation energy of antisites. Isotherms can be used to deduce the concentration of antisites on each sublattice at stoichiometry and for non-stoichiometric compositions. In
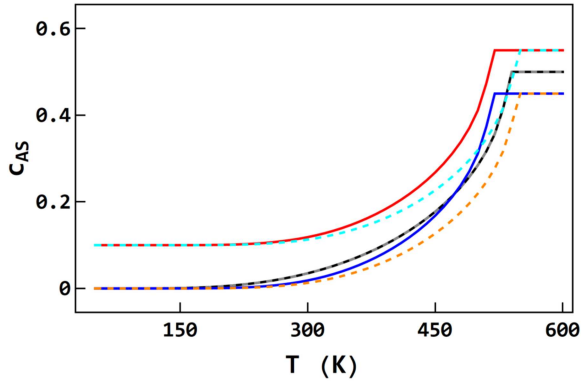
Figure 8. Antisites concentration as a function of T at different nominal concentration values surrounding the equiatomic composition ($c = 0.5$: $c_{AS(A)}$ black and $c_{AS(B)}$ grey; $c = 0.45$: $c_{AS(A)}$ blue and $c_{AS(B)}$ red; $c = 0.55$: $c_{AS(A)}$ cyan and $c_{AS(B)}$ orange).

the canonical ensemble, i.e. if the nominal concentration is imposed, the system forms pairs of antisites to accommodate the concentration (B atoms on the A-rich sublattice and A atoms on the B-rich sublattice). In the grand canonical ensemble, when the difference in chemical potential is imposed, antisites can be isolated on a single sublattice. In this last case, the formation of complexes with vacancies makes it possible to compensate a deviation in stoichiometry. The concentration of vacancies being much lower than that of antisites, especially at low temperatures, we neglect them.

$c_{AS(A)}$ and $c_{AS(B)}$ the concentration of antisites A (resp. B) on sublattice B (resp. A) verify $c_{AS(A)} = c_2$, and $c_{AS(B)} = 1 - c_1$ and are obtained by solving equation (14) for different compositions around stoichiometry.

Figure 8 shows two quite distinct regimes whatever the composition. There is an athermal regime at low temperatures where antisite concentrations vary only slightly. Then, there is a thermally activated regime at the highest temperatures characterized by a strong dependence of antisite concentrations with temperature. At the stoichiometric composition, there are as many antisites on the two sublattices and the concentration increases from 200 K. For a sub-stœchiometric composition the athermic plateau is a little longer. The concentration of antisites A on sublattice B is zero, while that of antisites B on sublattice A is non-zero. Concentrations of antisites A and B increase from 300 K faster than at stoichiometry. For an over-stoichiometric composition, the concentration of antisites B on sublattice A is zero, while that of antisites A on sublattice B is non-zero. Concentrations of antisites A and B increase from 300 K more slowly than at stoichiometry. This inversion is related to the evolution of $V_1^{L1_0}$ with concentration, for constant effective pair interactions the same increase with temperature is obtained regardless of the deviation from the stoichiometry considered.

In the literature, the concentration of antisites is often determined from the Wagner–Schottky model [33] whose central quantity is the enthalpy of formation of an antisite. We have previously shown that the permutation enthalpy that drives the phase diagram is made of three driving forces. One may

therefore wonder what are the driving forces for the enthalpy of antisite formation.

The enthalpies of antisite formation are written according to the permutation enthalpies of the corresponding sublattices:

$$\Delta H_{AS(A)}^{form} = \Delta H_2^{perm} - \Delta\mu \quad \text{et} \quad \Delta H_{AS(B)}^{form} = \Delta H_1^{perm} - \Delta\mu. \tag{15}$$

At low temperatures and at the stoichiometric composition $\Delta\mu = \left(\Delta H_1^{perm} + \Delta H_2^{perm}\right)/2$, which leads to:

$$\Delta H_{AS(A)}^{form} = \Delta H_{AS(B)}^{form} = \left(\Delta H_2^{perm} - \Delta H_1^{perm}\right)/2. \tag{16}$$

This equation allows to split the formation enthalpy of antisites according to the 3 components. It should be recalled that the cohesion effect, equal to the difference in the cohesion energies of the two species (equation (B.2a)), does not depend on the sublattice and this is also the case for the size effect (equation (B.2c)). Only the chemical component changes from one sublattice to another. The relationship (15) thus becomes

$$\Delta H_{AS(A)}^{form} = \Delta H_{AS(B)}^{form} = \left(\Delta H_{chem,2}^{perm} - \Delta H_{chem,1}^{perm}\right)/2. \tag{17}$$

While the permutation enthalpy is the result of the 3 effects of cohesion, alloy and size, the formation enthalpy of an antisite contains less information than the permutation enthalpy since it depends only on the alloying effect. The formation enthalpy of antisites only allows to deduce the number of antisites in the vicinity of the stoichiometry, it does not allow to get the isotherms, nor the phase diagram.

4. Conclusions

We develop an approach that describes the disordered system and apply it to a system which tends to form ordered structures at low temperatures. This new approach is complementary to the cluster expansion in the sense that all site energies are average quantities obtained after relaxation of the atomic positions.

In this work we have shown that this formalism predicts the hierarchy of ordered structures. The results are in good agreement with the direct calculations obtained with the semi-empirical interatomic potentials. For a given concentration, the distinction between the structures (DO_{22} and A_2B_2) is accurately obtained when the site energies take into account the chemical nature of the first and second neighbouring atoms. These results justify the use of site energies to study the alloy at low temperature when ordering occurs. We are aware that we have only tested a few structures. The extension to a large number of structures is an important task that will be the subject of future work.

Site energies constitute a very powerful tool for analyzing the thermodynamic driving forces contained in an energetic model for random solid solutions as well as for systems with short or long range ordering. The enthalpy of permutation is the central quantity that separates the cohesive, chemical and elastic effects. For an ordered system, the permutation enthalpy curve displays plateaux and steps. Each plateau corresponds to an almost linear variation in the concentration of one sublattice while the concentration of the other sublattices

remains constant. This behaviour is only due to the chemical effect. We have found that the creation of one antisite is at the origin of both the quasi-vertical step at a stoichiometric composition and the change of plateau. The permutation enthalpy and the formation enthalpy of antisites are linked. The enthalpy of formation of the antisites is less rich than the enthalpy of permutation because it only includes the chemical contribution.

Finally, the AuPd alloy is characterized by a competition between the chemical effect and the size effect. At low concentrations, the size effect is predominant and leads to a demixtion between a quasi-pure Pd phase and the ordered compound $AuPd_3$. At higher concentrations, the chemical effect predominates, leading to long range ordering.

Appendix A. Mean field approximation with LRO

The mean field modelling can be applied to ordered structures by considering sublattices, each sublattice being homogeneous. The Hamiltonian H of the system is expressed as the sum of each sublattice Hamiltonian H_i:

$$H = \frac{1}{nsr} \sum_{i=1}^{nsr} H_i, \quad (A.1)$$

where nsr is the number of sublattices and H_i is given by

$$H_i/N = c_i E_A^{\sum_{j=1,nsr} Z_{ij}c_j} + (1-c_i) E_B^{\sum_{j=1,nsr} Z_{ij}c_j}, \quad (A.2)$$

with c_i the concentration of the ith sublattice which is equal to $c_i = \frac{N_{Ai}}{N_i}$, N_{Ai} and N_i being respectively the number of A atoms and the number of sites of the ith sublattice. The nominal composition is related to the concentration of sublattices according to $c = \frac{\sum_{i=1}^{nsr} c_i}{nsr}$. Z_{ij} is the number of nearest bonds between sites of the ith sublattice and the jth sublattice (for $nsr = 4$, $Z_{ii} = 0 \; \forall i$ and $Z_{ij} = 4 \forall j \neq i$).

The free energy is $F = H - TS - \frac{N_{at}}{nsr} \left(\sum_{i=1}^{nsr} c_i \right) \Delta\mu$, with S the configurational entropy

$$S = \frac{1}{nsr} \sum_{i=1}^{nsr} S_i, \quad (A.3)$$

and the configurational entropy of the ith sublattice S_i is written in a classic manner in the form of

$$S_i/N_{at} = -k_B (c_i \ln(c_i) + (1-c_i) \ln(1-c_i)). \quad (A.4)$$

The minimization of free energy leads to the system of nsr non-linear equations coupled as follows:

$$\frac{c_i}{1-c_i} = \exp\left(-\frac{\Delta H_i^{perm} - \Delta\mu}{k_B T} \right), \quad (A.5)$$

with $\Delta H_i^{perm} = \frac{\partial H}{\partial N_{Ai}} = \frac{nsr}{N_{at}} \frac{\partial H}{\partial c_i}$. ΔH_i^{perm} is the permutation enthalpy of the ith sublattice i.e. the enthalpy balance during a permutation of one B atom of the ith sublattice into one A atom. ΔH_i^{perm} is composed of three terms:

$$\Delta H_i^{perm}(c) = \Delta H_{B\to A}(c) + \Delta H_n(c) + \Delta H_{\Delta c}(c), \quad (A.6)$$

where:

- $\Delta H_{i,B\to A}$ is the enthalpy change on the site where the exchange $B \to A$ (of the ith sublattice) occurs:
$$\Delta H_{B\to A} = E_A^{\sum_j Z_{ij}c_j} - E_B^{\sum_j Z_{ij}c_j};$$

- ΔH_n is the enthalpy change on all nearest-neighbors sites of the one on which the exchange $B \to A$ occurs: $\Delta H_n =$
$$\sum_{m\neq i} Z_{im} \left(c_m \left. \frac{\partial E_A^p}{\partial p} \right|_{\sum_j Z_{mj}c_j} + (1-c_m) \left. \frac{\partial E_B^p}{\partial p} \right|_{\sum_j Z_{mj}c_j} \right);$$

- $\Delta H_{\Delta c}$ is an elastic term related to the variation of the site energies for all sites due to the change in nominal concentration induced by the exchange $B \to A$:

$$\Delta H_{\Delta c} = \frac{1}{nsr} \sum_{m=1}^{nsr} \left(c_m \left. \frac{\partial E_A^p}{\partial c} \right|_{\sum_j Z_{mj}c_j} + (1-c_m) \left. \frac{\partial E_B^p}{\partial c} \right|_{\sum_j Z_{mj}c_j} \right).$$

We solve the system of equations via a damped-dynamics algorithm [43].

Appendix B. Driving forces with LRO

For RSS, the permutation enthalpy (given by equation (6)) can be written as the sum of 3 effects:

$$\Delta H_{coh}^{perm} = \left(E_A^Z(1) - E_B^0(0) \right), \quad (B.1a)$$

$$\Delta H_{chem}^{perm} = \left(E_A^{Zc}(c) - E_A^Z(c) \right) - \left(E_B^{Zc}(c) - E_B^0(c) \right) + Z \left(c \left. \frac{\partial E_A^p}{\partial p} \right|_{Zc} + (1-c) \left. \frac{\partial E_B^p}{\partial p} \right|_{Zc} \right), \quad (B.1b)$$

$$\Delta H_{size}^{perm} = \left(E_A^Z(c) - E_A^Z(1) \right) - \left(E_B^0(c) - E_B^0(0) \right) + \left(c \left. \frac{\partial E_A^p}{\partial c} \right|_{Zc} + (1-c) \left. \frac{\partial E_B^p}{\partial c} \right|_{Zc} \right). \quad (B.1c)$$

The cohesive term is the standard difference in cohesive energies between pure metals. The chemical contribution is related to the chemical local environment change. It can also be written $-Z(1 - 2c) V_1^X$. The size contribution is related to the change of lattice parameter with c.

In the case of LRO, we extend the rule of 3 effects to the permutation enthalpy of each sublattice: $\Delta H_i^{perm} = \Delta H_{coh,i}^{perm} + \Delta H_{chem,i}^{perm} + \Delta H_{size,i}^{perm}$ with:

$$\Delta H_{coh,i}^{perm} = \left(E_A^Z(1) - E_B^0(0) \right), \quad (B.2a)$$

$$\begin{aligned} \Delta H_{chem,i}^{perm} = & \left(\left(E_A^{\sum_j Z_{ij}c_j}(c) - E_A^Z(c) \right) - \left(E_B^{\sum_j Z_{ij}c_j}(c) - E_B^0(c) \right) \right) \\ & + \sum_{m\neq i} Z_{im} \left(c_m \left. \frac{\partial E_A^p}{\partial p} \right|_{\sum_j Z_{mj}c_j} + (1-c_m) \left. \frac{\partial E_B^p}{\partial p} \right|_{\sum_j Z_{mj}c_j} \right) \end{aligned} \quad (B.2b)$$

$$\Delta H_{\text{size},i}^{\text{perm}}$$
$$= \left(\left(E_A^Z(c) - E_A^Z(1) \right) - \left(E_B^0(c) - E_B^0(0) \right) \right)$$
$$+ \frac{1}{nsr} \sum_{m=1}^{nsr} \left(c_m \frac{\partial E_A^p}{\partial c} \bigg|_{\sum_j Z_{mj} c_j} + (1-c_m) \frac{\partial E_B^p}{\partial c} \bigg|_{\sum_j Z_{mj} c_j} \right) \tag{B.2c}$$

The cohesive and size effects are identical for each sublattice. The cohesive effect does not vary between the disordered and the ordered states. The elastic term differs slightly between the disordered and ordered states (due to the deviation between $\frac{\partial E_X^p}{\partial c}\big|_{Zc}$ and $\frac{\partial E_X^p}{\partial c}\big|_{\sum_j Z_{mj} c_j}$) but it can be numerically overlooked. The most changing driving force is the chemical effect.

Appendix C. Application to the L1$_0$

The L1$_0$ structure can be described by equations of appendix A with only 2 sublattices ($nsr = 2$, $Z_{ii} = 4$ et $Z_{ij} = 8$ with i and j =1 or 2).

Equation (A.6) become at the stoichiometric composition for ($c_1 = 1, c_2 = 0$):

$$\Delta H_1^{\text{B}\rightarrow\text{A}} = \left(E_A^{Z_{11}} - E_B^{Z_{11}} \right) + Z_{11} \frac{\partial E_A^p}{\partial p} \bigg|_{Z_{11}} + Z_{12} \frac{\partial E_B^p}{\partial p} \bigg|_{Z_{12}}$$
$$+ \frac{1}{2} \left(\frac{\partial E_A^p}{\partial c} \bigg|_{Z_{11}} + \frac{\partial E_B^p}{\partial c} \bigg|_{Z_{12}} \right) \tag{C.1a}$$

$$\Delta H_2^{\text{B}\rightarrow\text{A}} = \left(E_A^{Z_{21}} - E_B^{Z_{21}} \right) + Z_{21} \frac{\partial E_A^p}{\partial p} \bigg|_{Z_{11}} + Z_{22} \frac{\partial E_B^p}{\partial p} \bigg|_{Z_{21}}$$
$$+ \frac{1}{2} \left(\frac{\partial E_A^p}{\partial c} \bigg|_{Z_{11}} + \frac{\partial E_B^p}{\partial c} \bigg|_{Z_{21}} \right) \tag{C.1b}$$

One can thus write the permutation enthalpy of sublattice i as the sum of $\Delta H_1^{\text{B}\rightarrow\text{A}}$ and a complementary term (see equation (13a) and (13b)) by laying:

$$V_1^{\text{L1}_0}(c) = \frac{\partial E_A^p}{\partial p} \bigg|_{\sum_j Z_{1j} c_j} - \frac{\partial E_B^p}{\partial p} \bigg|_{\sum_j Z_{1j} c_j}. \tag{C.2}$$

Since figure 6 shows that the curvature can be neglected, we can consider the linear part of site energies, and thus:

$$\left(E_A^{Z_{11} c_1 + Z_{12} c_2} - E_A^{Z_{11}} \right) - \left(E_B^{Z_{11} c_1 + Z_{12} c_2} - E_B^{Z_{11}} \right)$$
$$= (Z_{11} c_1 + Z_{12} c_2) V_1^{\text{L1}_0}(c) - Z_{11} V_1^{\text{L1}_0}(c),$$

$$\left(E_A^{Z_{21} c_1 + Z_{22} c_2} - E_A^{Z_{21}} \right) - \left(E_B^{Z_{21} c_1 + Z_{22} c_2} - E_B^{Z_{21}} \right)$$
$$= (Z_{21} c_1 + Z_{22} c_2) V_1^{\text{L1}_0}(c) - Z_{21} V_1^{\text{L1}_0}(c).$$

For constant nearest-neighbour pair interactions, $E_A^p = p V_{\text{AA}}/2 + (Z-p) V_{\text{AB}}/2$ and $E_B^p = p V_{\text{BA}}/2 + (Z-p) V_{\text{BB}}/2$, then equation (C.1a) and (C.1b) become:

$$\Delta H_1^{\text{perm},0} = -4 V_1^{\text{Ising}} + 12\tau + \Delta H_{\Delta c}(c)|_0, \tag{C.3a}$$

$$\Delta H_2^{\text{perm},0} = +4 V_1^{\text{Ising}} + 12\tau + \Delta H_{\Delta c}(c)|_0, \tag{C.3b}$$

with $\Delta H_{\Delta c}(c)|_0$ the 3rd term on RHS corresponds to the elastic effect at the stoichiometry, $V_1^{\text{Ising}} = (V_{\text{AA}} + V_{\text{BB}} - 2 V_{\text{AB}})/2$ and $\tau = (V_{\text{AA}} - V_{\text{BB}})/2$.

In the ordered state, at the stoichiometry, the chemical potentials difference is given by $\Delta\mu = \Delta H^{\text{perm}}(c = 1/2) = \left(\Delta H_1^{\text{perm}} + \Delta H_2^{\text{perm}} \right)/2$. So it can be written as follow:

$$\Delta\mu = 12\tau + \Delta H_{\Delta c}(c)|_0 \tag{C.4}$$

The formation enthalpy of A antisites on the sublattice rich in B, $\Delta H_{\text{AS(A)}}^{\text{form}}$, and of B antisites on the sublattice rich in A, $\Delta H_{\text{AS(B)}}^{\text{form}}$, are $\Delta H_{\text{AS(A)}}^{\text{form}} = \Delta H_2^{\text{perm}} - \Delta\mu$ and $\Delta H_{\text{AS(B)}}^{\text{form}} = -\Delta H_1^{\text{perm}} + \Delta\mu$. Thus at the stoichiometry it leads to:

$$\Delta H_{\text{AS(A)}}^{\text{form}} = \Delta H_{\text{AS(B)}}^{\text{form}} = 4 V_1^{\text{Ising}} \tag{C.5}$$

The formation enthalpies of antisites are only depending on the effective pair interaction.

ORCID iDs

F Berthier https://orcid.org/0000-0003-3564-3930

References

[1] Senhaji A, Tréglia G and Legrand B 1994 *Surf. Sci.* **307–309** 440
[2] Berthier F, Legrand B and Tréglia G 1999 *Acta Mater.* **47** 2705
[3] Ducastelle F, Legrand B and Tréglia G 1990 *Prog. Theor. Phys. Suppl.* **101** 159
[4] Tréglia G, Legrand B and Ducastelle F 1988 *Europhys. Lett.* **7** 575
[5] Creuze J, Berthier F, Tétot R and Legrand B 2000 *Phys. Rev.* B **62** 2813
[6] Berthier F, Creuze J and Legrand B 2017 *Phys. Rev.* B **95** 224102
[7] Berthier F, Creuze J, Gabard T, Legrand B, Marinica M C and Mottet C 2019 *Phys. Rev.* B **99** 014108
[8] Connolly J W D and Williams A R 1983 *Phys. Rev.* B **27** 5169(R)
[9] Wolverton C, Ceder G, de Fontaine D and Dreyssé H 1993 *Phys. Rev.* B **48** 726
[10] Papaconstantopoulo D A and Mehl M J 2001 *Phys. Rev.* B **64** 172510
[11] Yu M, Trinkle D R and Martin R M 2011 *Phys. Rev.* B **83** 115113
[12] Zhu B, Front A, Guesmi H, Creuze J, Legrand B and Mottet C 2017 *Comput. Theor. Chem.* **1107** 49
[13] Haruta M, Yamada N, Kobayahsi T and Lijima S 1989 *J. Catal.* **115** 301
[14] Piccolo L, Piednoir A and Bertolini J C 2005 *Surf. Sci.* **592** 169
[15] Zhou Y, Wang S, Ding B and Yang Z 2007 *Catal. Lett.* **118** 86
[16] Darby J B Jr 1966 *Acta Metall.* **14** 265
[17] Okamoto H and Massalski T B 1985 *Bull. Alloy Phase Diagrams* **6** 229
[18] Barabash S V, Blum V, Muller S and Zunger A 2006 *Phys. Rev. B Condens. Matter* **74** 035108

[19] Sluiter M H F, Colinet C and Pasturel A 2006 *Phys. Rev. B Condens. Matter* **73** 174204

[20] Kanamori J and Kakehashi Y 1977 *J. Phys. Colloq.* **38** 274

[21] Atanasov I and Hou M 2009 *Surf. Sci.* **603** 2639

[22] Shan B, Wang L G, Yang S, Hyun J, Kapur N, Zhao Y J, Nicholas J B and Cho K 2009 *Phys. Rev. B Condens. Matter* **80** 035404

[23] Nelayah J, Nguyen N T, Alloyeau D, Wang G Y and Ricolleau C 2014 *Nanoscale* **6** 10423

[24] Nagasawa A 1964 *J. Phys. Soc. Jpn.* **19** 2345

[25] Nagasawa A, Matsuo Y and Kakinoki J 1965 *J. Phys. Soc. Jpn.* **20** 1881

[26] Matsuo Y, Nagasawa A and Kakinoki J 1966 *J. Phys. Soc. Jpn.* **21** 2633

[27] Kawasaki Y, Ino S and Ogawa S 1971 *J. Phys. Soc. Jpn.* **30** 1758

[28] Asta M, Foiles S M and Quong A A 1998 *Phys. Rev. B* **57** 11265

[29] Korzhavyi P A, Ruban A V, Lozovoi A Y, Vekilov Y K, Abrikosov I A and Johansson B 2000 *Phys. Rev. B* **61** 6003

[30] Neumayer M and Fahnle M 2001 *Phys. Rev. B* **64** 132102

[31] Song X L, Zhang J M and Xu K W 2007 *J. Alloys Compd.* **436** 23

[32] Besson R, Legris A and Morillo J 2006 *Phys. Rev. B* **74** 094103

[33] Wagner C and Schottky W 1931 *Z. Phys. Chem.* B **11** 163

[34] Hagen M and Finnis M W 1998 *Philos. Mag.* **77** 447

[35] Ruban A V, Popov V A, Portnoi V K and Bogdanov V I 2014 *Philos. Mag.* A **94** 20

[36] Bragg W L and Williams E J 1934 *Proc. R. Soc.* A **145** 699

[37] Ruban V I 2014 *Philos. Mag.* **94** 1192

[38] Foiles S M 1985 *Phys. Rev. B* **32** 7685

[39] Rosato V, Guillopé M and Legrand B 1989 *Philos. Mag.* A **59** 321

[40] Bitzek E, Koskinen P, Gälher F, Moseler M and Gumbsch P 2006 *Phys. Rev. Lett.* **97** 170201

[41] Shockley W 1938 *J. Chem. Phys.* **6** 130

[42] Finel A and Ducastelle F 1986 *Europhys. Lett.* **1** 135

[43] Khoutami A, Legrand B and Tréglia G 1993 *Surf. Sci.* **287/288** 851